J. Fluid Mech. (1991), *vol.* 224, *pp.* 579–599
Printed in Great Britain

Evolution and dynamics of shear-layer structures in near-wall turbulence

By ARNE V. JOHANSSON[1], P. HENRIK ALFREDSSON[1]† AND JOHN KIM[2]

[1] Department of Mechanics, Royal Institute of Technology, S-100 44 Stockholm, Sweden
[2] NASA Ames Research Center, Moffet Field, CA 94035, USA

(Received 7 December 1989)

Near-wall flow structures in turbulent shear flows are analysed, with particular emphasis on the study of their space–time evolution and connection to turbulence production. The results are obtained from investigation of a database generated from direct numerical simulation of turbulent channel flow at a Reynolds number of 180 based on half-channel width and friction velocity. New light is shed on problems associated with conditional sampling techniques, together with methods to improve these techniques, for use both in physical and numerical experiments. The results clearly indicate that earlier conceptual models of the processes associated with near-wall turbulence production, based on flow visualization and probe measurements need to be modified. For instance, the development of asymmetry in the spanwise direction seems to be an important element in the evolution of near-wall structures in general, and for shear layers in particular. The inhibition of spanwise motion of the near-wall streaky pattern may be the primary reason for the ability of small longitudinal riblets to reduce turbulent skin friction below the value for a flat surface.

1. Introduction

In the flow visualization study on transition to turbulence in pipe flow Reynolds (1883) was able to observe large-scale structures in the turbulent flow by use of a simple but ingenious technique. He visualized the flow by injecting dye in the centre of the pipe and observed the flow with a short electrical spark in a dark room, thus enabling him to get an *instantaneous* picture of the flow. His observations indicated that the flow, to a large extent, consisted of relatively regular large-scale eddies. During the first half of the twentieth century these results were more or less overlooked when the statistical theory of turbulence was developed together with laboratory investigations of turbulence statistics using mainly hot-wire anemometry. One exception was the work in Göttingen (see e.g. Prandtl & Tietjens 1934) where structures of different propagation velocities were selectively visualized by long-time exposures of floating particles on the surface of an open surface channel with a camera moving with a chosen speed. These studies revealed the existence of fairly large-scale and persistent flow structures. A series of pioneering flow visualization experiments carried out at Stanford University (Kline *et al.* 1967; Kim, Kline & Reynolds 1971) changed the course of turbulence research, and established the

† Present address: Department of Gasdynamics, Royal Institute of Technology, S-100 44 Stockholm, Sweden.

importance of organized, deterministic structures for turbulence production. The hydrogen-bubble technique used by the Stanford group made it possible to continuously observe the formation of various structures in the flow. The use of low-speed water channels of large dimensions made it possible to reach fairly large viscous lengthscales, which in turn made observations in the viscous sublayer possible. This region was shown to consist of neighbouring elongated regions of high and low velocity, where the low-speed regions intermittently were lifted from the wall out into the buffer region. The visual observations also indicated subsequent oscillations and violent break-up of the flow into small scales. This process, which was observed to occur suddenly and abruptly was referred to as *bursting*, and was found to be coupled to a large part of the turbulence production. Also, the trace particle visualization study of Corino & Brodkey (1969) confirmed much of the details observed by Kline *et al.*

The realization that intermittent processes are important in turbulent flows made it necessary to develop new techniques for data evaluation. Conditional sampling, in the meaning of ensemble averaging of important structures or parts of the flow, was introduced, at first by analogue means, for example by opening an analogue gate when the measured signal fulfils some chosen condition. One of the first of these investigations was carried out by Kovasznay, Kibens & Blackwelder (1970) who studied the intermittent region at the boundary-layer edge, trying to distinguish between the potential flow regions and the turbulent bulges and to make averages of mean velocity and r.m.s. levels within the two flow regions. Today, conditional sampling is done with computers, through analysis of long-time records of velocity or pressure signals. In this way, various detection conditions may be tried, and the effect of parameter settings can be tested. One should keep in mind, though, the inherent subjectivity resulting from the choice of detection criteria. Since the outcome is, more or less strongly, coupled to these criteria, one should always make some kind of estimate of the dynamical importance of the structures in question, for example in terms of contribution to the overall Reynolds stress.

The creation of internal inclined shear-layer structures is perhaps the dominating feature of the near-wall flow field. It results from the lift-up (often referred to as an ejection, if it is rapid) of fluid from low-speed streaks in the viscous sublayer. These buffer-region shear layers are highly three-dimensional and are inclined at a relatively shallow angle with respect to the wall. The strength and inclination is affected by the shearing action of the mean velocity gradient. At maximum strength the instantaneous gradient is often close to that of the mean gradient at the wall. A fixed observer will consequently see a high value of the temporal derivative, and a large change, of the streamwise velocity as it passes by. This feature of the *bursting sequence* is utilized in the so called VITA (variable interval time averaging) technique which has been used in various experimental investigations (see e.g. Blackwelder & Kaplan 1976; Johansson & Alfredsson 1982) to detect shear-layer structures in boundary layers and channel flows. With this detection scheme (analysed in detail in, e.g. Johansson & Alfredsson 1983; Alfredsson & Johansson 1984) an event is considered to occur when the variance of u averaged over a *short* time T exceeds a chosen threshold level, k, times the long-time-averaged variance (i.e. the mean-square value of the streamwise fluctuations). The detection position is normally chosen in the buffer region. Many other methods have been developed (see, e.g. Lu & Willmarth 1973; Brodkey, Wallace & Eckelmann 1974) to focus on different stages of development in this process or other aspects coupled to near-wall turbulence production. A comparison between results obtained with a number of different

detection schemes was carried out by Bogard & Tiederman (1986) through use of simultaneous visualization and probe measurements.

Various investigations, using probe measurements, have confirmed the finding from flow visualizations that a large portion of the turbulence production occurs during highly intermittent events. The mean time between consecutive events as registered by a fixed probe (i.e. in an Eulerian reference frame) has been found to be much larger than the duration of individual events. Hence, turbulence production was concluded to be strongly intermittent both in time and space. One should, however, bear in mind the inherent difficulty in flow visualization, using hydrogen bubble, dye or other techniques, in following a specific structure or process for long times since all path lines diverge rapidly in a turbulent flow. Also, the structure need not be simply advected, but may propagate in a somewhat wave-life manner through the action of the pressure. Large contributions to the Reynolds stress have mainly been found to be directly associated with the lift-up of low-speed fluid, i.e. on the downstream side of the shear-layer structure. Thus the formation and evolution of shear-layer-like structures in the near-wall region of turbulent flows have been recognized to be intimately coupled to turbulence production.

A conceptual model of the various stages of the bursting process was put forward by Kline *et al.* (1967) and has remained a cornerstone in the perception of turbulence production in wall-bounded flows. A central part of the model is the localized lift-up of fluid from low-speed regions in the viscous sublayer into the buffer region, creating strong, more or less symmetric (with respect to the spanwise centre of the low speed region), internal shear layers coupled to a velocity profile with inflexional character. The flow visualization results indicated that a major portion of the turbulence production occurs during violent break-up of the flow structure into small scales, which was believed to originate from an inflexional instability giving rise to a growing oscillation of the lifted low-speed region. The conceptual model does not, however, account for regeneration of the low-speed regions in the viscous sublayer.

The development of simulation methods for turbulent flows has revolutionized the work carried out on detection of turbulence producing events. Probe methods have in a few investigations been used to map spatial features of the structures (e.g. Johansson, Alfredsson & Eckelmann 1987*a*; Wark 1988; Guezennec & Choi 1989). However, a complete space–time mapping in three dimensions by experimental means would be an almost impossible task, in particular in the innermost portions of the flow, such as the viscous sublayer and the buffer region. At low Reynolds numbers in simple geometries the use of databases generated from direct numerical simulations has become a feasible alternative, where three-dimensional mapping of all components of the velocity field is relatively straightforward. In fact experiments at low Reynolds numbers (at least in channel geometry) are almost pointless today. The physical and *numerical* experiments instead complement each other, and the importance of simulations will certainly grow with the increase in computer power. This also calls for some redirection of experimental efforts towards complex geometries and high-Reynolds-number (near-wall) investigations. For investigations at low Reynolds numbers that require extremely long time series or many realizations, such as ensemble averaging of turbulent spots, experimental methods will continue to be the only realistic alternative. Also, fairly little is known about turbulence in *non-canonical* situations, i.e. in situations with surface roughness, surface curvature, strong pressure gradients, etc.

The present work is directed towards the analysis of near-wall flow structures in turbulence, with particular emphasis on the study of their space–time evolution and

connection to turbulence production. Dynamics and evolution, which are key issues here, are both aspects that are extremely difficult to address in an experimental investigation. The possibility of investigating the features of structures at different stages of development is in practice unique to *numerical experiments*. The database studied here represents data from direct numerical simulation of turbulent channel flow, but most of the conclusions are believed to be also valid for other types of wall-bounded shear flows. Detection of buffer region shear-layer structures was done with a spatial counterpart to the VITA technique. Also, various aspects of conditional sampling schemes will be analysed, and improvements such as *phase jitter* removal and centring are investigated. The work reported here summarizes and extends work carried out during the first and second Summer Programs (1987 and 1988) of the Centre for Turbulence Research at NASA Ames–Stanford (Johansson, Alfredsson & Kim 1987*b*; Alfredsson, Johansson & Kim 1988). New ideas about the asymmetry of near-wall flow structures are also presented that suggest a need for modification of the earlier conceptual model of the bursting process.

2. The database

The numerical database from which the present results were obtained was generated at NASA Ames from direct numerical simulations of turbulent channel flow at a Reynolds number (R_*) of 180 based on friction velocity (u_τ), channel half-height (b) and kinematic viscosity (ν). For the analysis, 47 different flow fields separated by three viscous time units were used, where each field had all primary flow variables at two million grid points, i.e. $128 \times 129 \times 128$ points in the streamwise (x), wall-normal (y) and spanwise (z) directions. The spatial resolution was 17.67 and 5.89 viscous units in the x- and z-directions, respectively. The resolution in the y-direction varied with the distance from the wall, and corresponded to 0.05 at the wall and 4.4 viscous units at the channel centreline. The fluctuating parts of the velocities in the x-, y- and z-directions and the pressure will be denoted by u, v, w and p, and superscript $+$ will denote normalization with inner (viscous) scales.

Comparisons between results from full numerical simulations obtained with the Ames code and experimental data have been presented elsewhere. Results for all basic statistical quantities have been shown to agree well with channel flow data from the Göttingen oil channel for computations with a total number of 4 million modes (Kim, Moin & Moser 1987). The present database was computed with half that number of modes, but has been verified to yield essentially identical results.

A possibly interesting smaller difference (that probably cannot be explained by spatial resolution effects) between the simulation results and available experimental data concerns the maximum streamwise r.m.s. velocity, which occurs around $y^+ = 15$. In this region we expect wall similarity to hold for all fluctuating quantities. However, the amplitude of this maximum varies greatly between different experimental investigations, as has been shown by for example Zaric (1972). To a large extent these differences can be attributed to inappropriate measurement techniques, especially the use of too large sensors which give spatial resolution problems.

Johansson & Alfredsson (1983) compiled results for the maximum of $u_{\rm rms}/u_\tau$ from a number of investigations and plotted the maximum r.m.s. value as function of the probe length in viscous units. This work was later extended by Ligriani & Bradshaw (1987) who also tested various length-to-diameter ratios. The data from different investigations essentially collapsed onto a single curve when plotted as function of

probe length in viscous units, and the results indicate a true value of approximately 2.9 for the maximum of $u_{\rm rms}/u_\tau$. LDV measurements, which are not affected by the spanwise scale as they are taken on individual particles, by Luchik & Tiederman (1985) show a maximum value of 2.8, whereas a value of about 2.7 is found in the simulations (Kim *et al.* 1987; Gilbert 1988). For hot wires the expansion of the response equation has been carried to higher orders and the statistics needed to evaluate the error terms have been obtained from numerical simulations. However, this has shown that these terms are much too small to explain the difference. Instead, the explanation appears to be a fairly strong Reynolds-number dependence at very low Reynolds numbers, as indicated by some recent simulation results (Spalart 1988).

3. Results

3.1. *Detection of near-wall flow structures*

Detection of flow structures associated with large amounts of turbulence production by means of probe methods is by no means a trivial matter. Events occurring at regular intervals in a flow field would be detectable by a frequency analysis of the velocity signal. However, as soon as there is phase jitter affecting the occurrence, ordinary frequency analysis loses much of its value. A number of detection schemes have been developed and used to detect coherent flow structures in wall-bounded shear flows. Most of them are one-point methods that make use of either the streamwise velocity or the uv-product. Even if a perfect one-point detection method were available which detects all events passing the probe without giving rise to any false detections, there would still be several types of difficulties in obtaining accurate conditional averages of the various flow variables associated with the structure under study. One source of error in the quantitative estimates of conditional averages is the phase jitter, i.e. the differences in time and/or space separation between the detection point and for example the location of the maximum associated uv-peak for the individual events. This type of problem has been addressed by for example Blackwelder (1977) and Johansson, Her & Haritonidis (1987*c*). The latter used a cross-correlation technique between the individual events and the ensemble average, which was shown to be quite effective in removing the phase jitter, and resulted in, among other things, a substantially increased amplitude of the wall-pressure peak associated with the structure.

With one-point detection methods different events may be detected at quite different positions along the span of the structure. This *space jitter* leads to smearing of the ensemble averages and to quantitative errors in the velocity and Reynolds stress amplitudes. The variation normal to the wall, of course, also varies somewhat between individual structures. In the experimental situation the remedy for the space jitter problem would be multi-point detection. Although some recent experimental efforts have been devoted to multi-point detection methods (see for example Komori, Murakami & Ueda 1989), this is considerably easier to achieve with computer-generated numerical databases.

The results presented in the following concerning near-wall shear-layer structures were obtained by use of the VISA technique (Kim 1985), which is a spatial counterpart to the VITA technique. The temporal averaging is here replaced by averaging over a streamwise length L in the construction of the local variance of the streamwise fluctuations. Modifications of the previously used VISA technique such as spanwise centring of individual structures and phase jitter removal were applied

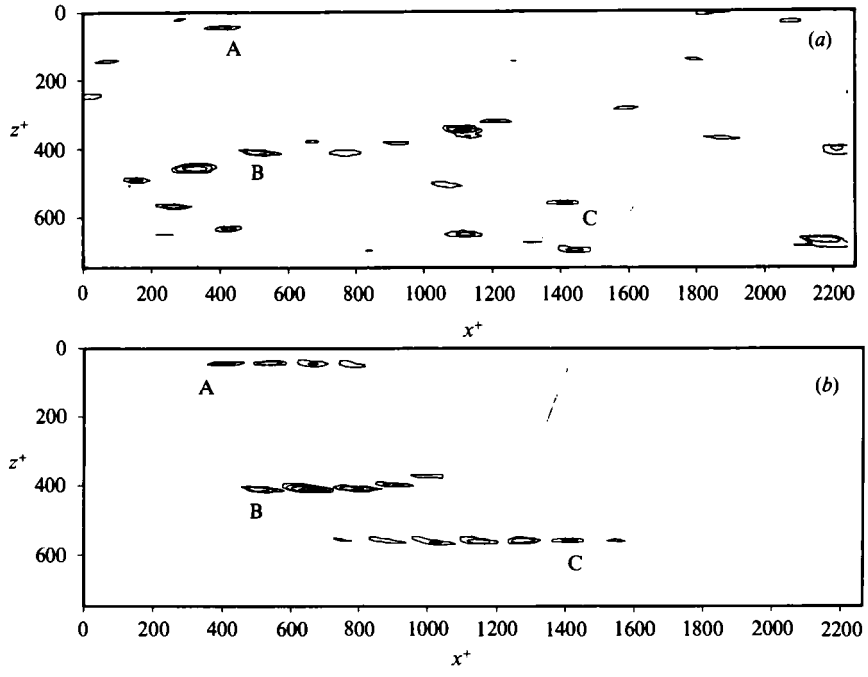

FIGURE 1. Contours of the normalized streamwise velocity variance averaged over a distance, L, of 200 viscous length units at $y^+ = 15$. Contours start at 1.0 with an increment of 0.5. (*a*) All events at a chosen time. (*b*) The space–time development of the variance associated with the events marked A, B and C in (*a*). Time separation between plots is 12 viscous time units.

in the present work, and will be described in conjunction with the results presented below. A modified VISA scheme is also introduced in which spanwise asymmetric features of the detected structures are retained.

3.2. *Statistics of near-wall flow structures*

For the bulk of the results presented in the following, detection was triggered when the VISA-variance (normalized by $u^2_{\rm rms}$) at $y^+ = 15$ exceeded a threshold (k) of 1.0. The regions of high values of the locally averaged variance (or VISA-variance), thus indicating the existence of shear-layer structures, give a spatially spotty picture in the buffer region. In figure 1 the variance was averaged over about 200 viscous length units (11 grid points) in the x-direction, and about 30 regions with levels above 1.0 can be observed (figure 1*a*). In the present approach these regions were identified, i.e. their maxima were located and followed from their formation to their disappearance, for a period of 138 viscous time units (t_*), with a separation of 3 viscous time units between the analysed flow fields. In this way the events become centred in the spanwise direction before, for example, ensemble averaging is applied, and it is ensured that each individual structure will be counted only once. The space–time history of each island (i.e. shear layer) could be constructed from the 47 consecutive flow fields. This would in practice be impossible to construct from experimental data.

As examples, the space–time history of three high-variance islands marked by A, B and C is shown in figure 1 (*b*), where consecutive plots are separated by $12t_*$. Event C is here followed over more than $70t_*$ during which it has travelled approximately 900 viscous units, corresponding to 5 channel half-heights. The shear layer can, however, be identified over considerably larger distances. The mean survival time of

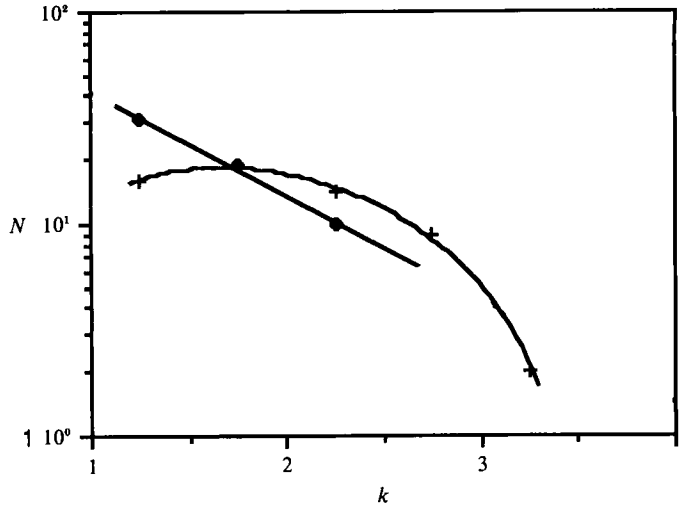

FIGURE 2. Number of detected events as a function of the threshold level ($L = 200$ viscous units, $y^+ = 15$). Squares represent events at a chosen time and plus signs represent the *amplitudes* for the same events when they are individually traced to locate their maximum.

the shear layers, such as those indicated in figure 1, was approximately $50t_*$, but some strong shear layers could be followed throughout the entire extent of the time studied ($138t_*$).

If the events in figure 1 (*a*), and those detected at $y^+ = 15$ near the opposite wall, are divided into intervals of the maximum variance amplitude, the low amplitudes will dominate, i.e. at a given time there are many events (regions of high variance) with a maximum variance just above the threshold (figure 2). On the other hand, if all these events are traced in time to locate the time of maximum shear-layer strength (i.e. global variance maximum), the most probable variance maximum is instead found in the interval 1.5–2.0, and values close to 3.5 were observed. As should be expected, the strong shear layers could be followed over longer times than the weaker ones.

The propagation velocity of the shear layers could be determined from their space–time history, and was found to be $10.6u_\tau$ with a standard deviation of $\pm 1.0u_\tau$. This is substantially lower than the value, $13.0u_\tau$, obtained from an experimental investigation (Johansson *et al.* 1987*a*) at about the same Reynolds number (10% higher). In that study the VITA-detection was carried out at $y^+ = 15$ and a second probe was positioned at various y- and x-positions downstream of the detector probe (e.g. at $y^+ = 20$). However, the averaging time was $10t_*$, which would correspond to a shorter averaging length than that used in the analysis of the numerical data. Also, there is an inherent difference between spatial and temporal data evaluation. It is here noteworthy that the propagation velocity of high-amplitude wall-pressure fluctuations has been found (experimentally) to be roughly 12 in wall units (see for example Schewe 1983). The lateral movement of the structures was normally found to be rather undramatic as illustrated by the examples in figure 1 (*b*).

The significance of these flow structures for the flow dynamics in the near-wall region depends on their frequency of occurrence (or probability of occurring within a given area). In order to enable comparisons with experimental results obtained with a stationary probe the average number of detections per z-position was determined and normalized by the streamwise extent of the domain (2260) divided

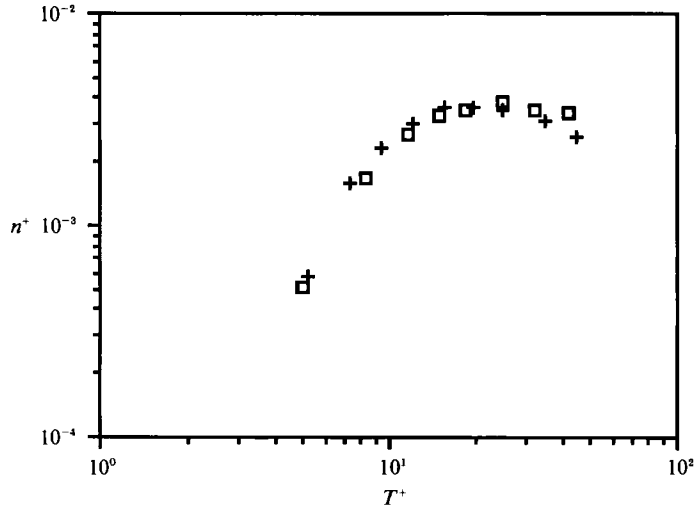

FIGURE 3. Number of events that would be detected per unit time with a stationary probe as a function of the averaging time: simulation (□) and measurements in the Göttingen oil channel (+) at about the same Reynolds number ($k = 1.0$, $y^+ = 15$).

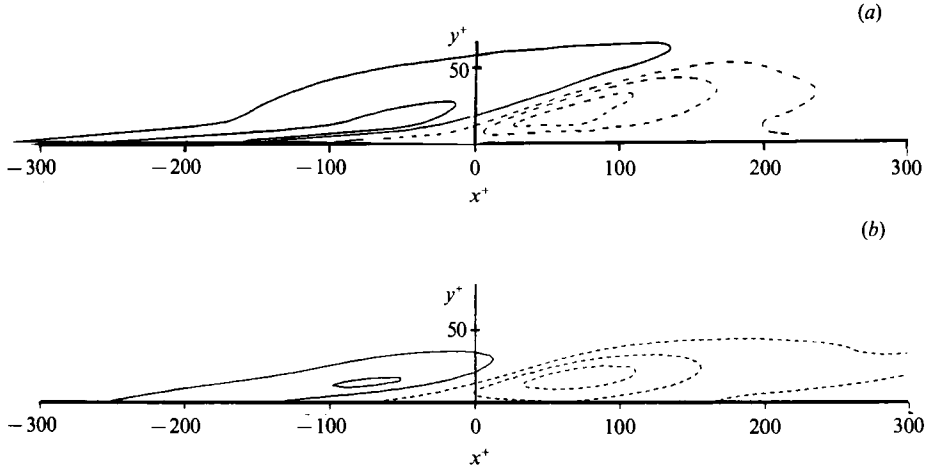

FIGURE 4. Conditionally averaged shear-layer structure in the near-wall region of channel flow. Comparison of streamwise velocity disturbance ($\langle u \rangle / u_{\mathrm{rms}}(y)$) in the mid (x, y)-plane for (*a*) experimental results at $Re_\tau = 200$ (Johansson *et al.* 1987*a*, events detected by VITA with $T = 10$ and $k = 1.0$) and (*b*) simulation results at $Re_\tau = 180$ (detected with $L = 200$ and $k = 1.0$). Solid and broken lines denote positive and negative contours, respectively.

by the propagation velocity (10.6). This means that a shear layer, if signified by a region of high variance extending over several z-positions, is counted several times. This procedure yields a result equivalent to the number of detections per unit time for a fixed probe. Also, the averaging length was converted to an equivalent averaging time by use of the propagation velocity. The agreement is excellent (see figure 3) between the present results obtained in this manner and the experimental results (unpublished results by Johansson, Alfredsson & Eckelmann). One should bear in mind that the scaling used is immaterial since the Reynolds number is approximately the same for the two data sets.

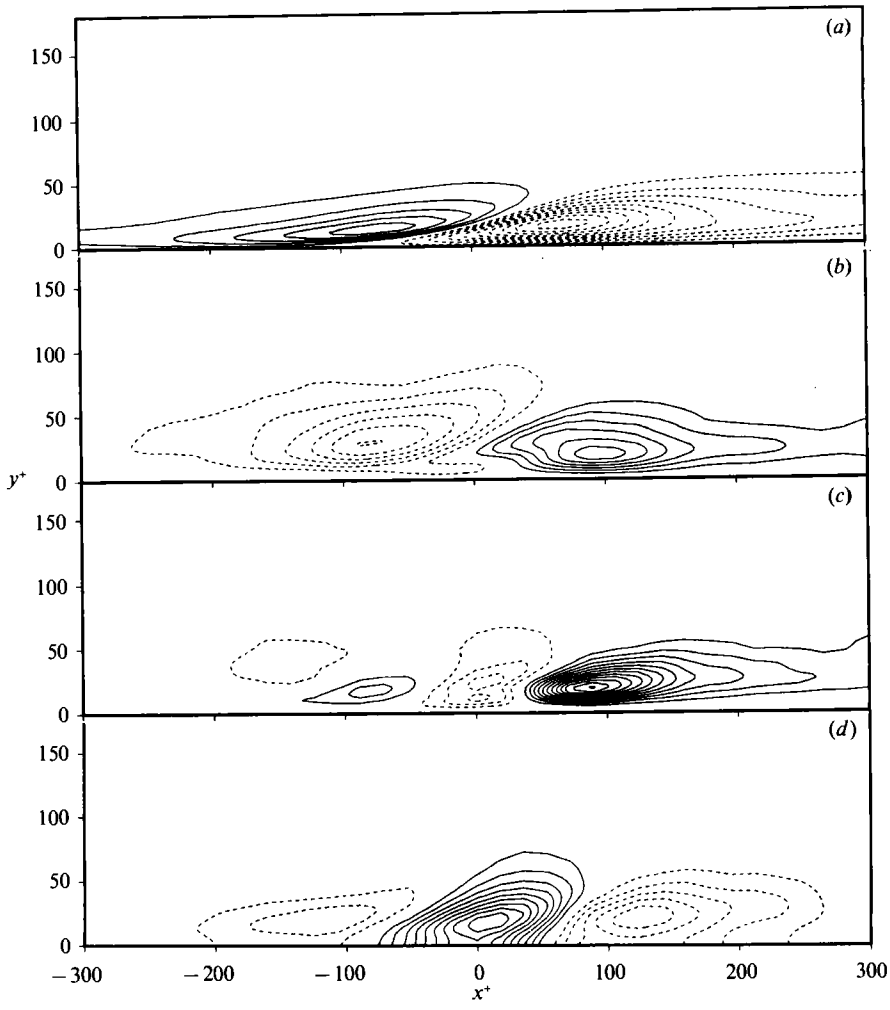

FIGURE 5. Ensemble averaged VISA-events detected with $L = 200$ and $k = 1.0$. Solid and broken lines denote positive and negative contours, respectively. (*a*) $\langle u\rangle/u_\tau$, contour increment is 0.5; (*b*) $\langle v\rangle/u_\tau$, contour increment is 0.1; (*c*) $\langle uv-\overline{uv}\rangle$, contour increment = 0.2, (*d*) $\langle p-\bar{p}\rangle$ contour increment = 0.2.

3.3. *Spatial structure and characteristics of near-wall shear layers*

Johansson *et al.* (1987*a*) determined the spatial characteristics in the (x, y)-midplane of near-wall shear-layer structures from two-probe measurements. The conditionally averaged isocontours of the normalized disturbance velocity, $\langle u\rangle/u_{\rm rms}$, from that investigation (figure 4*a*) show good agreement with the computed results of the present study (figure 4*b*). Hence, the results from the physical and numerical experiments describe the same dynamics, as we should expect since the Reynolds number is approximately the same in these two channel flows. In the numerical experiment 60 events, detected at both sides of the channel at one time step, were used in the ensemble averaging, which involves centring of the individual realizations in both the x- (as in conventional conditional averaging) and the z-directions. Hence, boxes 600 long, 200 wide and 180 high (the entire half-channel height) centred around the point of maximum variance (at $y^+ = 15$) are averaged. In the following,

absolute scaling of the conditional averages (denoted by $\langle\ \rangle$), i.e. normalization by u_τ (or other appropriate viscous scales), will be used.

Conditional averages of u, v, $uv-\overline{uv}$ and the fluctuating pressure in the (x, y)-midplane are shown in figure 5 (all normalized by inner scales). They were obtained from the numerical data in a manner similar to that which would be used in an experimental situation, although here spatial averages are obtained, and spanwise centring is used, which would require multiprobe measurements in an experiment. An interesting feature is that close to the wall the lifted low-speed fluid is pushed back towards the wall, resulting in a so-called wall-ward interaction. This is in close agreement with the observations of Eckelmann *et al.* (1977). It is also quite evident that there is strong streamwise shear associated with the detected structure and that the regions of coherent velocity are confined below a y^+ of about 50.

From analysis of databases for boundary-layer flows at three Reynolds numbers (for details see Johansson *et al.* 1987*b*), it was found that the overall size of the structures in viscous units increased slowly with increasing Reynolds number.

The maximum deviation from the long-time mean on the low-speed side of the shear-layer in figure 5(*a*) is almost twice as large as that on the high-speed side. Similarly the amplitude of the normal velocity is also much higher on the downstream side, which also gives a strong uv-peak in that region (figure 5*c*). The uv-contribution on the upstream side is practically negligible at this z-location.

The corresponding results in the (x, z)-plane, supplemented with the $\langle w \rangle$ pattern, are shown in figure 6 for $y^+ = 15$. The spanwise scale of the primary low- and high-speed regions is seen to be about 50, which is the same as the distance between high- and low-speed streaks in the viscous sublayer.

Spanwise centring of the events was found to be essential to obtain reasonable quantitative estimates of the associated Reynolds stress contributions. Without such centring the resulting maximum uv is drastically reduced (by roughly 50%) on the ejection side. It should be noted here that (to the present authors' knowledge) all previous results, experimental as well as numerical, presented in the literature has been obtained without proper centring. The reduced amplitudes without spanwise centring can be attributed to the resulting jitter in the spanwise separation between the uv-peak and the detector position, and to the fact that the spanwise scale of the uv-peak is rather small.

The pressure patterns (figures 5*d* and 6*e*) associated with the shear-layer structure exhibit several interesting features. The wall pressure, which is not shown here but is very similar to that at $y^+ = 15$, shows a positive peak over a region roughly 100 viscous units long and 50 units wide immediately beneath and around the centre of the shear layer, where somewhat of a high-pressure ridge can be observed. The highest pressure amplitudes are found in the middle of the shear layer at about $y^+ = 15$, whereas surrounding this central region there is a low-pressure domain, in which the largest amplitudes are found on the downstream side. The shape of the high-pressure regions as seen in figures 5(*d*) and 6(*e*) closely conforms to that of the dominating high-pressure structures in the near-wall region as observed by Robinson, Kline & Spalart (1989) in simulated visualizations of numerically computed boundary-layer flow.

The general characteristics, such as streamwise extent in viscous units, of the wall-pressure pattern also agree closely with earlier reported experimental results obtained in pipe and boundary-layer flows (see for example Langeheineken 1981; Dinkelacker & Langeheineken 1983; Kobashi & Ichijo 1986; Johansson *et al.* 1987*c*). However, the peak amplitude in the present case is only a fraction, approximately

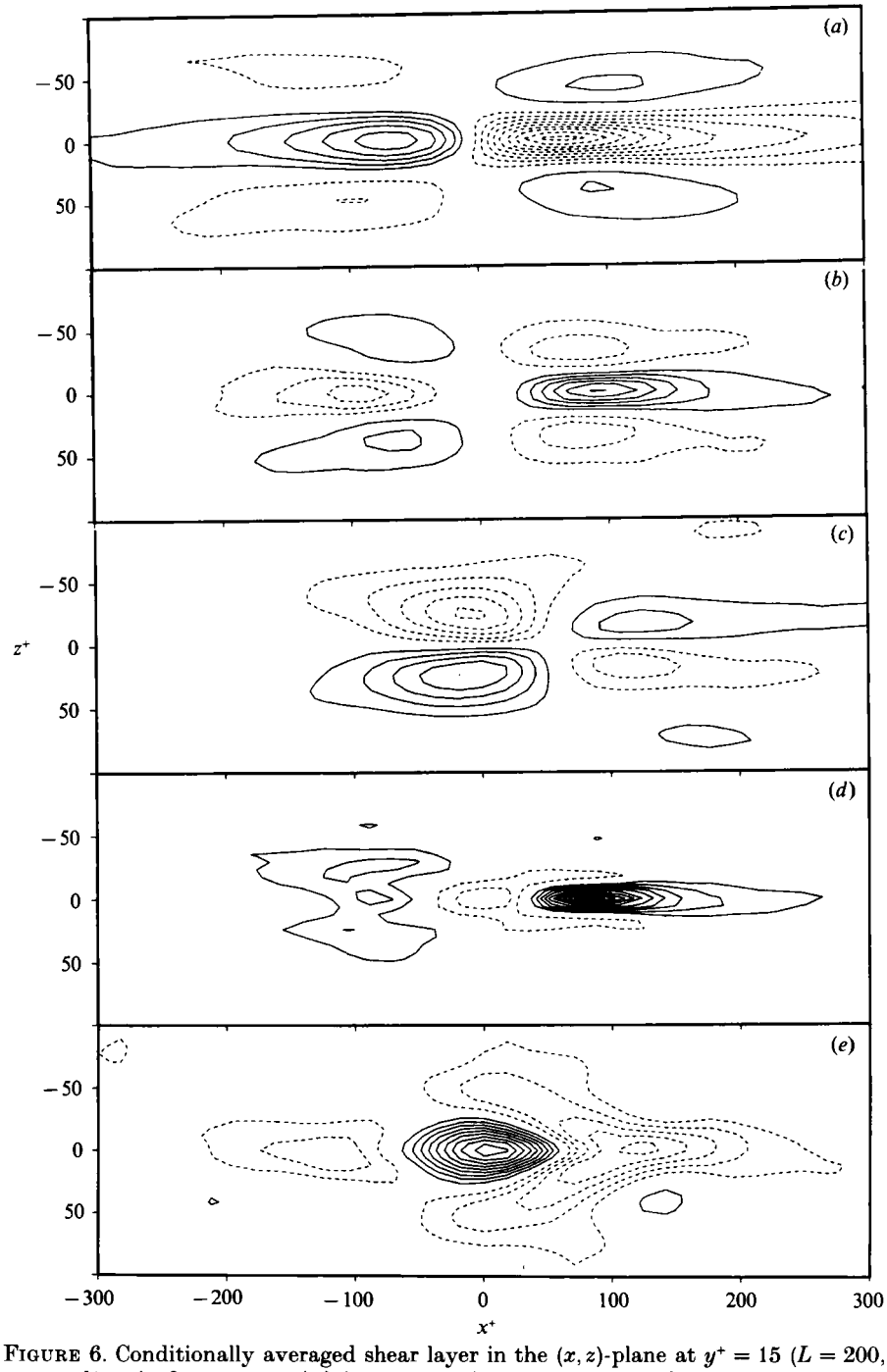

FIGURE 6. Conditionally averaged shear layer in the (x, z)-plane at $y^+ = 15$ ($L = 200$, $k = 1$). (a, b) as in figure 5; (c) $\langle w \rangle / u_\tau$, contour increment = 0.2; (d) as in 5(c); (e) as 5(d).

one third, of that obtained experimentally in a high-Reynolds-number boundary-layer flow (cf. figure 7 of Johansson *et al.* 1987*c*). This conclusion refers to an amplitude scaled in inner variables, and it is interesting to note that the amplitudes become comparable when normalized by the r.m.s.-value. One should here also note

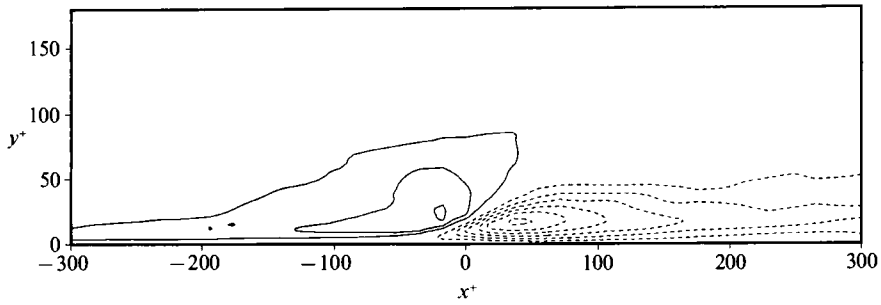

FIGURE 7. Conditional average of u/u_τ in the mid (x, y)-plane obtained by pressure-peak detection at $y^+ = 15$ with a threshold level of $3.0p_{\rm rms}$. Contour increment = 0.5.

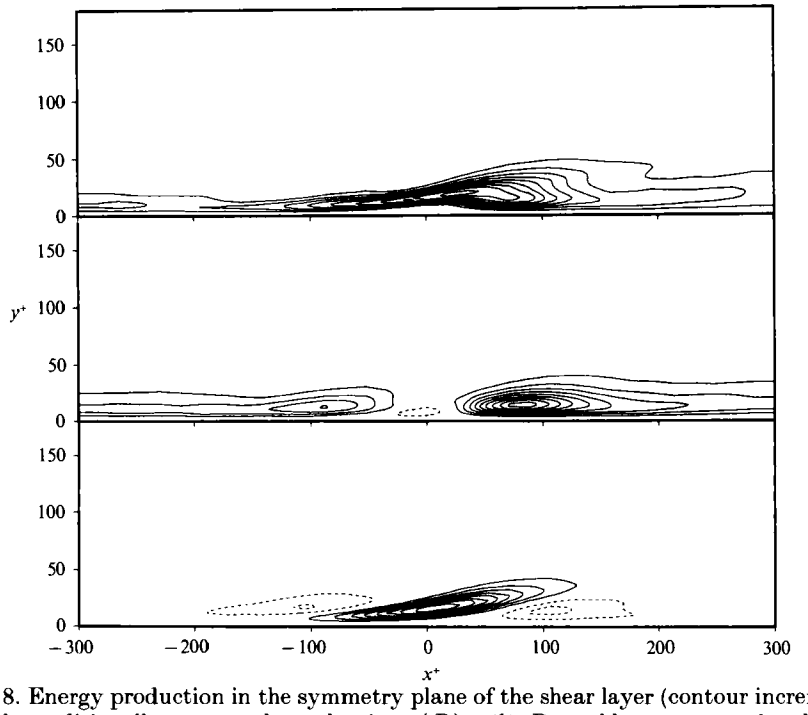

FIGURE 8. Energy production in the symmetry plane of the shear layer (contour increment = 0.1): (*a*) total conditionally averaged production $\langle P \rangle$; (*b*) Reynolds-stress-associated production $\langle -uv \rangle \mathrm{d}U/\mathrm{d}y$; (*c*) $\langle P \rangle - \langle -uv \rangle \mathrm{d}U/\mathrm{d}y$.

that the r.m.s.-value of the wall pressure normalized by $\tau_{\rm w}$ (≈ 1.43) is quite small (less than half) compared with the experimental results at higher Reynolds numbers, while the r.m.s.-value normalized by the centreline dynamic pressure is in fair agreement with experimental findings. This signifies a rather strong Reynolds-number dependence of $p_{\rm rms}/\tau_{\rm w}$ in the low-Reynolds-number regime (see also Spalart 1988).

An interesting detail is that the r.m.s.-value of the pressure fluctuations is larger in the buffer region than at the wall, reaching a maximum of about 1.8 at $y^+ = 30$. This behaviour is hence similar to that of the conditionally averaged pressure field, which may be taken as an indication that these structures are dominant contributors to the pressure field in the near-wall region.

The correspondence between high-pressure peaks in general and peaks associated

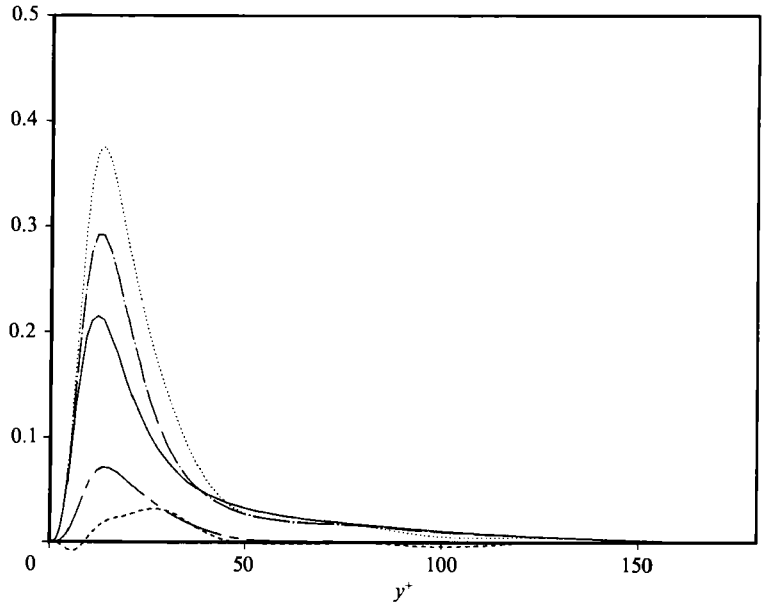

FIGURE 9. Energy production averaged over an area of 300×40 viscous units (x and z extent, respectively) around the centre of events: —, $-\overline{uv}\,\mathrm{d}U/\mathrm{d}y$; ···, $\langle P\rangle$; -·-·-; $\langle -uv\rangle\,\mathrm{d}U/\mathrm{d}y$; – – –, $-\overline{u^2}\langle\partial u/\partial x\rangle$; -·—·-, $-\overline{uv}\langle\partial u/\partial y\rangle$.

with shear-layer structures can be clearly illustrated by results from the use of a simple detection scheme triggering on local pressure levels above a chosen threshold. The similarity between the conditionally averaged u-pattern, in figure 7, obtained by applying this method at $y^+ = 15$ with a threshold level set at $3.0p_{\mathrm{rms}}$, and that obtained with the VISA technique (figure 5*a*) is obvious.

A key issue for the importance of coherent structures is their role in the turbulence production process. One can show that the conditionally averaged production of turbulent kinetic energy for a plane two-dimensional flow can be written

$$\langle P\rangle = -\langle uv\rangle\frac{\mathrm{d}U}{\mathrm{d}y} - \overline{u^2}\left\langle\frac{\partial u}{\partial x}\right\rangle - \overline{uv}\left(\left\langle\frac{\partial u}{\partial y}\right\rangle + \left\langle\frac{\partial v}{\partial x}\right\rangle\right) - \overline{v^2}\left\langle\frac{\partial v}{\partial y}\right\rangle - \overline{w^2}\left\langle\frac{\partial w}{\partial z}\right\rangle. \tag{1}$$

The first term on the right-hand side of (1) is the only one that remains in the long-time averaged sense. However, the total conditionally averaged production (figure 8*a*) is substantially higher than can be accounted for by this term (figure 8*b*). This is mainly due to strong gradients in the x- and y-directions of the conditionally averaged streamwise velocity (figure 8*c*). The largest of these terms is the second term in (1), which is illustrated in figure 9 where the production terms have been averaged over an area of 300×40 viscous units (streamwise and spanwise extent, respectively). This means that approximately 25% of the total area is covered by these *event areas* at any given time. Integrating the conditional production out to $y^+ = 30$ gives an average over this volume that is almost twice as large as the long-time mean value. This means that there is a factor of three between the production per unit volume within these regions of shear-layer activity and the rest of the volume below $y^+ = 30$. Also, the dissipation of turbulent energy was computed and found to be quite large in the vicinity of the shear-layer. It is noteworthy here that the conditionally averaged $\partial u/\partial z$ is not present on the right-hand side of (1). Hence, although high values of the spanwise gradient of u exist at the edges of the shear

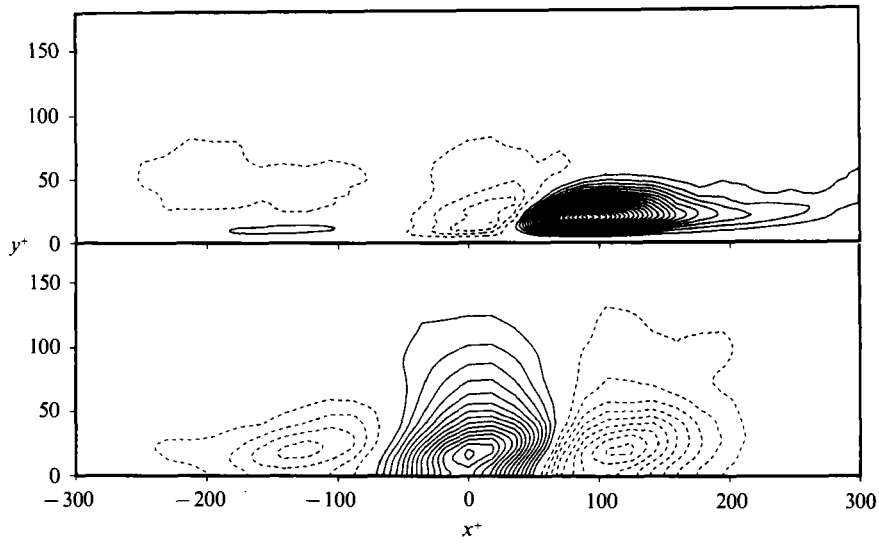

FIGURE 10. Enhanced conditional averages of Reynolds stress and pressure obtained by use of the cross-correlation technique (to be compared with figures 5c, d): (a) $\langle uv-\overline{uv}\rangle$, (b) $\langle p-\bar{p}\rangle$ (contour increment = 0.2).

layers they do not in themselves imply contributions to the associated turbulence production.

The use of correlation techniques to enhance the conditional averages, in the sense of removing phase (or here rather space) jitter, was also tried, and the results for the ensemble-averaged uv and pressure patterns are shown in figure 10. In this alignment procedure the ordinary conditional average was first constructed, whereafter each individual realization was cross-correlated with this average. Shifts in the x- and z-directions were determined before constructing the *enhanced* average. The maximum of $\langle uv-\overline{uv}\rangle$ on the downstream side of the shear layer increased by about 100% as a result of the alignment. The results for $\langle p-\bar{p}\rangle$ are similar. The clear dominance of the downstream quadrant-two type of motion for the contribution to the turbulence production (at least in the mid (x,y)-plane) becomes even more obvious. The results in this figure are also crucial for the interpretation of the quantitative results for Reynolds stress contributions, etc. Bogard & Tiederman (1987) studied the characteristics of ejections in channel flow through use of combined visualization and probe measurement techniques. They also observed the sensitivity to phase alignment in the conditional averaging procedure, and that intense ejections were associated with strong velocity gradients.

3.4. *Space–time development of near-wall flow structures*

By following all events that could be detected, with a VISA-threshold of 1.0, at a chosen time (i.e. from the two $y^+ = 15$ planes of a specific flow field) over their lifetime, the space–time position at which they reach their maximum strength (here taken as their maximum variance) could be located. These space–time positions were then used to construct conditional averages of events at their individual maximum strength. Similarly, conditional averages could be constructed at other stages of development. Conditional averages of u and uv at three different stages of development, namely at maximum strength (max. variance) and two stages, here referred to as *early* and *late*, are shown in figure 11. These stages were obtained by

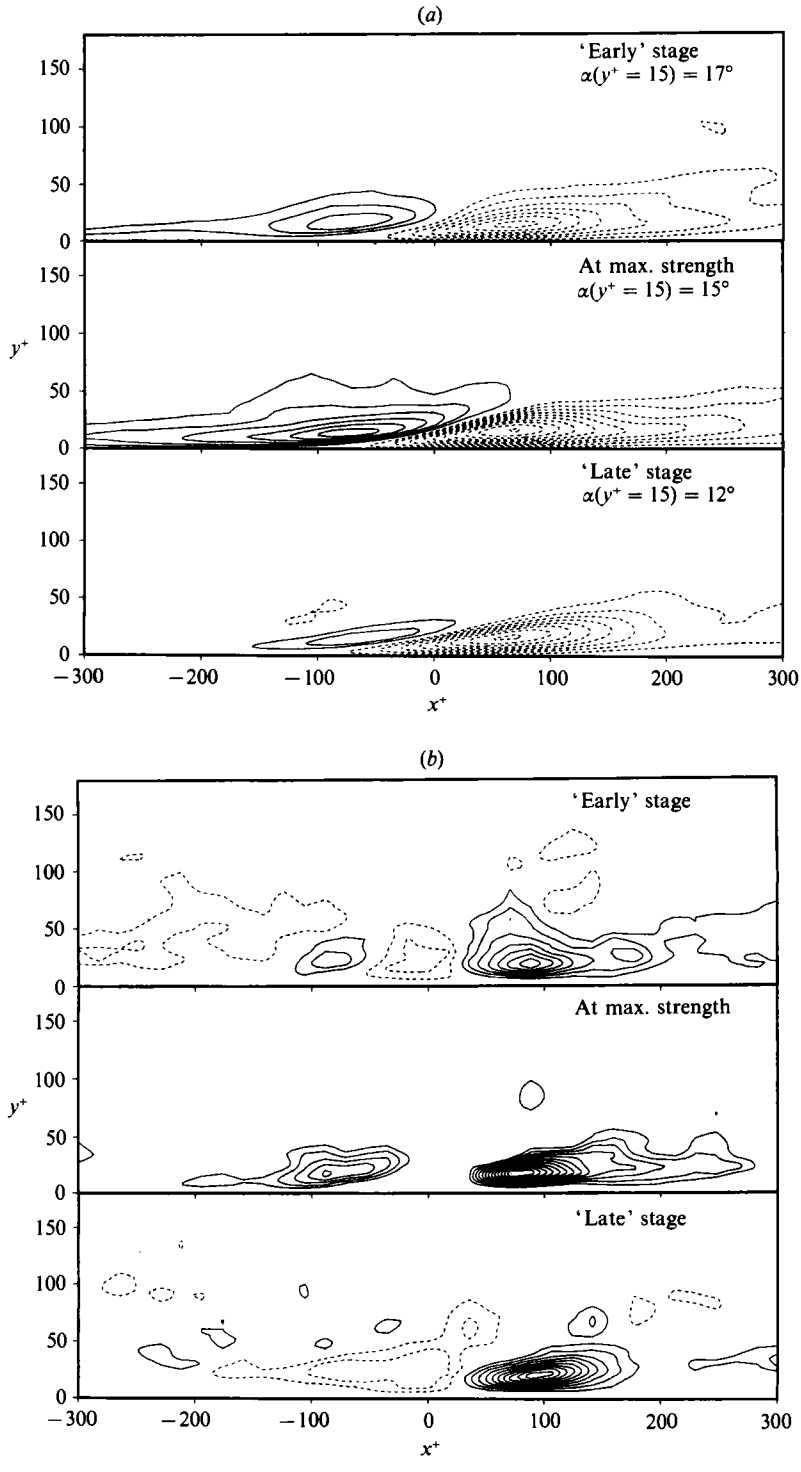

FIGURE 11. Conditional averages at three stages of development, where early and late refer to stages where the events are traced backwards or forwards in time until they attain an amplitude corresponding to a local variance of $0.7u_{\text{rms}}^2$ (primary detection with $L = 200$, $k = 1$). (*a*) $\langle u \rangle / u_\tau$, contour increment is 0.5; (*b*) $\langle uv - \overline{uv} \rangle$, contour increment = 0.2.

following the events backward and forward, respectively, in time to the instant when the local maximum variance is $0.7u_{\rm rms}^2$. The shear-layer inclination angle was found to decrease from 17° to 12° over this period of time (figure 11*a*). This manifestation of the *ageing* of the structure is a result of stretching by the mean shear. At maximum strength we observe large deviations from the mean velocity, as large as $5u_\tau$ on the downstream side at $y^+ \approx 20$. On this side of the shear layer the amplitudes are persistently large throughout the development, whereas on the upstream side the disturbance velocities tend to vanish much more quickly. A comparison with the results of Kreplin & Eckelmann (1979) may here be interesting. They determined a front structure from long-time correlation measurements between a probe in the viscous sublayer and one further out, and found a front angle of roughly 10° at $y^+ = 15$.

This situation is similar for the conditionally averaged v-velocity (not shown here), although here at the early stage the angle separating positive and negative v is as large as about 45° (cf. figure 5*b*) and the decrease in angle is more accentuated than for $\langle u \rangle$. The v-amplitudes on the two sides of the shear layer are comparable at the early and maximum strength stages, but here also the disturbance tends to vanish for large times on the upstream side. This gives some interesting features of the conditionally averaged uv-patterns at the different stages of development (figure 11*b*). From conventional probe methods, as well as from visualizations it has been concluded that the Reynolds stress contributions occur intermittently. From the present results it appears clear that, although spatially *spotty*, the Reynolds stress contribution from the downstream side of the shear layer stems, in the Lagrangian frame of reference, from a persistent motion of low-speed fluid away from the wall. Indeed, the associated $\langle uv \rangle$ could, on average, be followed several hundred viscous length units, and sometimes up to at least 1000 viscous units.

In order to investigate the generality of this conclusion, tracing of uv-peaks in general was applied. The persistence could be verified, and the *mean survival distance*, defined as the travelling distance over which the amplitude exceeded $4u_{\rm rms}v_{\rm rms}$, was about 300 viscous units for second-quadrant type of motions. The average propagation velocity was found to be slightly lower than that of the shear layers.

The time history of the peak variance amplitude was found to be quite symmetric about the time of maximum strength. An important observation, based on this and other results, was that no signs of small-scale oscillatory motions, or *violent break-up* could be observed in conjunction with the later stages of development, a conclusion that was also supported by inspection of a large number of individual realizations. This is in contrast to older conceptual models of the bursting process (Kline *et al.* 1967), and indicates the need for revision of the picture of near-wall turbulence production.

The associated pressure patterns undergo a development where an intense localized high-pressure region around and beneath the centre of the shear layer is found around the stage of maximum strength. At this stage the maximum amplitude is about $2.9\tau_{\rm w}$, or almost $2p_{\rm rms}$, above the mean pressure. These strong localized high-pressure regions could be of importance for boundary-layer noise generation.

3.5. *Asymmetric features of near-wall flow structures*

In conventional conditional averaging procedures, with or without spanwise centring, symmetric patterns are the result of homogeneity of the flow in the spanwise direction. It would result from any one-point detection method using the u- and/or v-velocity. Instantaneous shear-layer structures, on the other hand, often

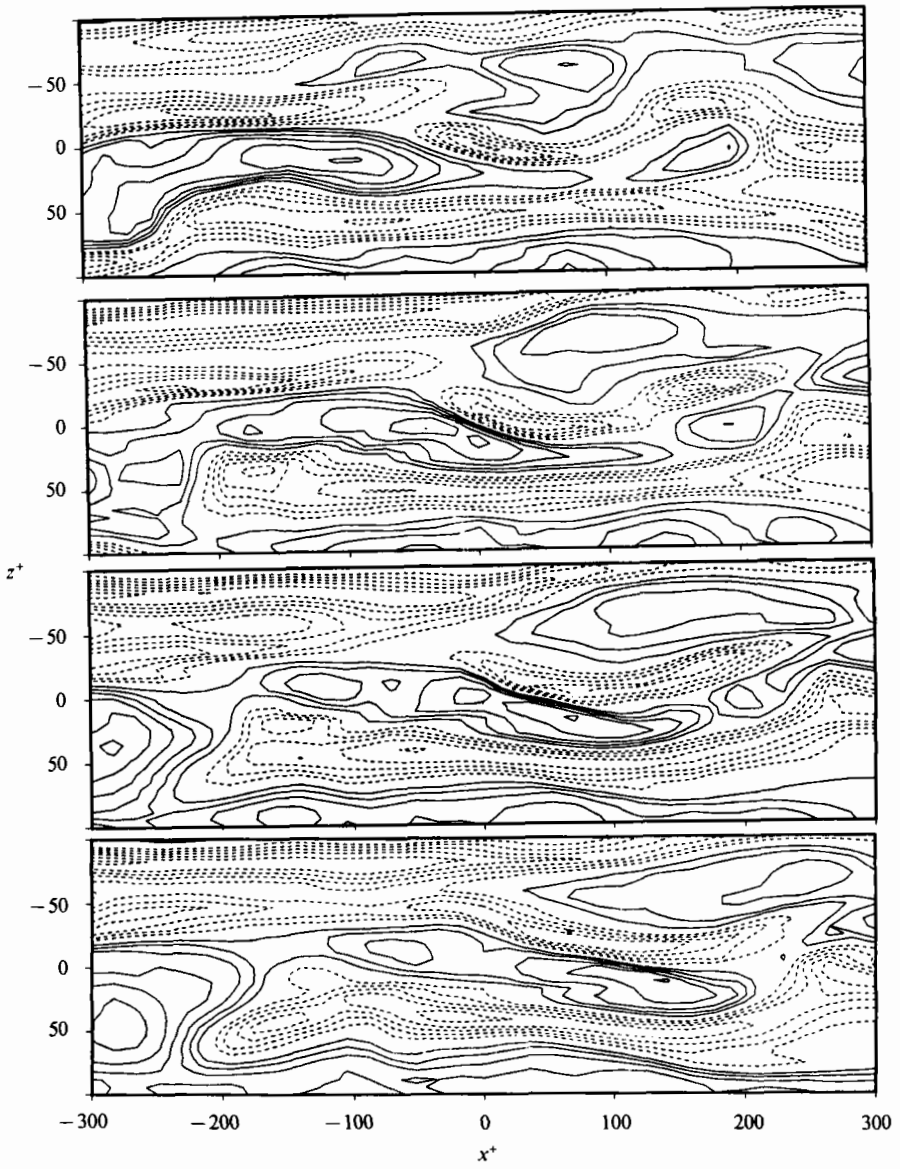

FIGURE 12. (x, z)-Plane contours of instantaneous u, for event B in figure 1, followed in time. Time increment between plots is 12 viscous units.

tend to develop strong asymmetries as they propagate downstream. The shear is often generated in a process where neighbouring elongated high- and low-speed regions interact through a localized spanwise motion, thus generating a flow structure with strong spanwise asymmetry. This can give large values of the spanwise gradient of the streamwise velocity at the centre of the shear layer. The average of the (absolute) spanwise gradient at the detection point for the events shown in figures 5 and 6 was found to be as large as 60% of the local mean velocity gradient. Asymmetric structures were in fact found to be more probable than symmetric ones.

The often-occurring asymmetric features of the shear layers is illustrated by the

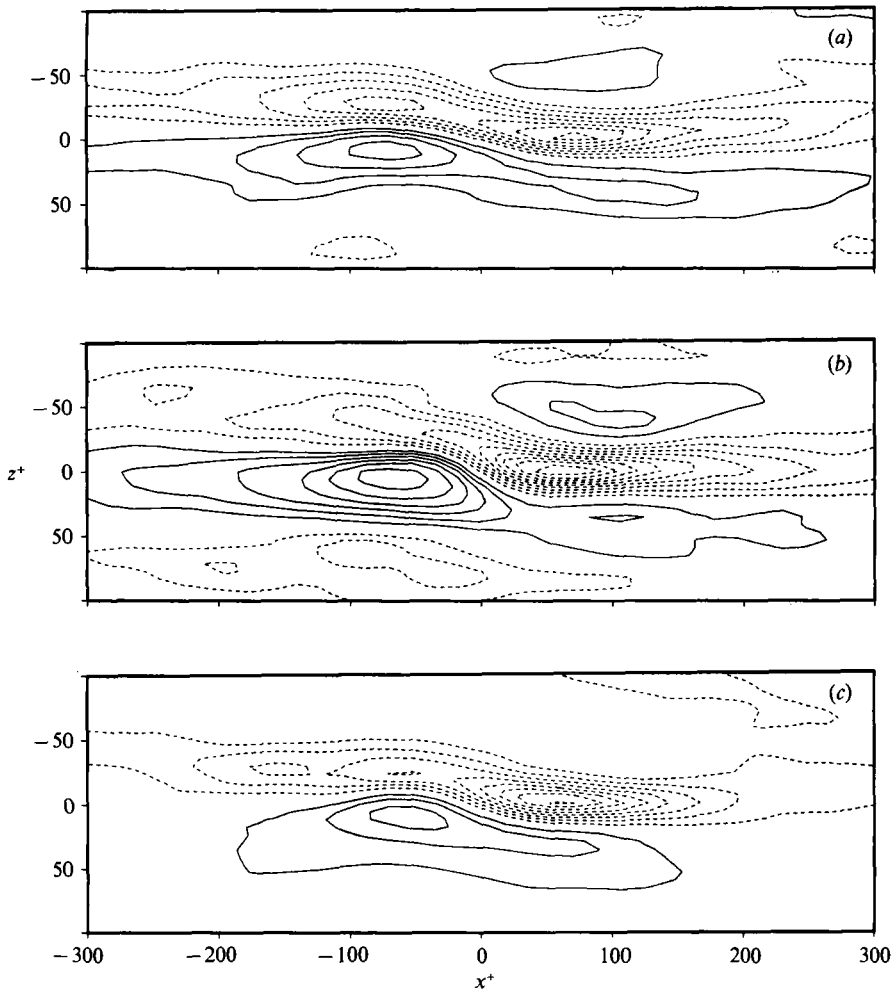

FIGURE 13. $\langle u \rangle / u_\tau$ at $y^+ = 15$ for three stages of development, obtained with the VISA technique modified to retain asymmetry features ($L = 200$, $k = 1$, contour increment = 0.5). (*a*) Early, (*b*) max. strength and (*c*) late stages, respectively.

space–time development of a single event in figure 12, where the frame of reference is chosen so that the centre of the shear layer is stationary. Here, only the planar (x, z) view is shown, which illustrates a meandering of the high- and low-speed regions, resulting in steep streamwise and spanwise gradients. The corresponding development as seen in the (x, y)-plane essentially only shows the steepening of the gradients in the shear layer.

In order to retain the spanwise asymmetry in the conditional average, a conditional sampling scheme was constructed that preserved the asymmetric features of the individual events, simply by switching the individual structure with respect to the (x, y)-midplane (and reversing the sign of w), according to the sign of the spanwise derivative of u at the detection point. The resulting averages at $y^+ = 15$ for different stages of development (figure 13) illustrate a mechanism for creation of high streamwise gradients through spanwise motions of the high- and low-velocity regions. Such streamwise gradients play a relatively important role in the generation of conditionally averaged turbulence production in that normal stress production is

of magnitude comparable with the regular shear production in the conditionally averaged sense (see figures 8 and 9). The asymmetry is strongest at maximum strength of the shear layer. This is an indication of the importance of spanwise asymmetry in these processes and suggests a picture of how near-wall flow structures develop and of how turbulence is produced which is quite different from the currently generally accepted picture. A simple mechanistic model of near-wall structures that describes much of the essential development characteristics of asymmetric structures has been developed by Landahl (1990).

The significance of the asymmetric structures was verified from the probability density distribution of $|\partial u/\partial z|$ at the detection point, which was found to be substantially wider than the normal one. The average value of $|\partial u/\partial z|$ at the detection point was found to be about twice the overall average at $y^+ = 15$. Similar signs of asymmetric flow structures have been found by Guezennec, Piomelli & Kim (1989), also from analysis of numerical databases.

4. Conclusions

The use of numerical databases generated through direct simulations of turbulent channel flow has given new insight into various aspects of the dynamics of near-wall turbulence, and has shed some new light on problems associated with conditional sampling techniques, and methods to improve these techniques, for use both in physical and numerical experiments. The main results obtained in the present study are summarized in the following.

The results, such as the lack of a violent break-up stage, clearly indicate that earlier conceptual models of the processes associated with near-wall turbulence production, based on flow visualization and probe measurements, need to be modified. Also, the development of asymmetry in the spanwise direction seems to be a major element in the evolution of near-wall structures in general, and for shear layers in particular.

Shear-layer structures are prevalent and persistent features of the near-wall region, and were shown to be important contributors to turbulence production. Individual structures were found to often have many features in common with the conditional averages obtained with the VITA or VISA methods.

Associated with the shear-layer structure is an intense localized high-pressure pattern, which could be of importance for boundary-layer noise generation and boundary-layer control.

The dominant associated uv-contribution was found to be caused by an ejection type of motion on the downstream side of the shear layer. This was particularly clear after *phase alignment* in the conditional averaging procedure.

Individual shear layers often develop a strong asymmetry as they propagate downstream. This feature is lost in conventional averaging procedures. From the evolution of the asymmetric structures it was found that the streaky pattern remains more or less intact after the most active stages of the process. This indicates that there may not be a need for a further regeneration process for the low- and high-speed streaks. The spanwise asymmetry is dynamically important in that it often appears to be directly coupled to the creation of the strong shear in the y-direction. A possibly important interpretation of these results is that manipulation of the near-wall flow structures in a way that inhibits spanwise motion, and development of spanwise asymmetries, should be effective in inhibiting the near-wall turbulence production process. This may be the primary reason for the ability of longitudinal small riblets

to cause turbulent drag reduction. It may here be interesting to note that Djenidi *et al.* (1989) observed *stabilization* of streaks over riblet surfaces in visualization experiments. Choi (1989) studied flow over riblet and smooth surfaces and suggested that the main mechanism for riblet drag reduction is related to restriction of spanwise motion of pairs of longitudinal vortices, resulting in a weak *premature burst*. The conclusion that spanwise motion is of central importance for riblet drag reduction is in accordance with the present findings, although pairs of longitudinal vortices were not observed to be a primary ingredient in this scenario. Since shear-layer structures also are associated with large-amplitude pressure peaks, inhibition of spanwise motion of the streaks and thereby inhibition of the sharpening of the shear layers may also be hypothesized to be effective for reducing boundary-layer noise.

Financial support from the Center for Turbulence Research and from the Swedish State Board for Technical Development for the two Swedish authors is gratefully acknowledged. We also wish to thank Professors Dan Henningson and Mårten Landahl for many fruitful discussions.

REFERENCES

ALFREDSSON, P. H. & JOHANSSON, A. V. 1984 On the detection of turbulence-generating events. *J. Fluid Mech.* **139**, 325.

ALFREDSSON, P. H., JOHANSSON, A. V. & KIM, J. 1988 Turbulence production near walls, the role of flow structures with spanwise asymmetry. In *Proc. Second Summer Program of the Center for Turbulence Research, Rep.* CTR-S88. NASA Ames/Stanford University.

BLACKWELDER, R. F. 1977 On the role of phase information in conditional sampling. *Phys. Fluids* **20**, S232.

BLACKWELDER, R. F. & KAPLAN, R. E. 1976 On the wall structure of the turbulent boundary layer. *J. Fluid Mech.* **76**, 89.

BOGARD, D. G. & TIEDERMAN, W. G. 1986 Burst detection with single-point velocity measurements. *J. Fluid Mech.* **162**, 389.

BOGARD, D. G. & TIEDERMAN, W. G. 1987 Characteristics of ejections in turbulent channel flow. *J. Fluid Mech.* **179**, 1.

BRODKEY, R. S., WALLACE, J. M. & ECKELMANN, H. 1974 Some properties of truncated turbulence signals in bounded shear flows. *J. Fluid Mech.* **63**, 209.

CHOI, K. S. 1989 Near-wall structure of a turbulent boundary layer with riblets. *J. Fluid Mech.* **208**, 417.

CORINO, E. R. & BRODKEY, R. S. 1969 A visual investigation of the wall region in turbulent flow. *J. Fluid Mech.* **37**, 1.

DINKELACKER, A. & LANGEHEINEKEN, T. 1983 Relations between wall-pressure fluctuations and velocity fluctuations in turbulent flow. In *Proc. Structure of Turbulent Shear Flow, IUTAM Symp., Marseille 1982.* Springer.

DJENIDI, L., LIANDRAT, J., ANSELMET, F. & FULACHIER, L. 1989 About the mechanism involved in a turbulent boundary layer over riblets. In *Proc. Second European Turbulence Conference, Berlin Sept. 1988* (ed. H. H. Fernholz & H. E. Fiedler). Springer.

ECKELMANN, H., NYCHAS, S. G., BRODKEY, R. S. & WALLACE, J. M. 1977 Vorticity and turbulence production in pattern recognized turbulent flow structures. *Phys. Fluids* **20**, S225.

GILBERT, N. 1988 Numerische Simulation der Transition von der laminaren in die turbulente Kanalströmung. Ph.D. thesis, University of Karlsruhe.

GUEZENNEC, Y. G. & CHOI, W. C. 1989 Stochastic estimation of coherent structures in turbulent boundary layers. In *Proc. Zoran Zaric Memorial Intl Seminar on Near-Wall Turbulence, May 1988 Dubrovnik.* Hemisphere.

GUEZENNEC, Y. G., PIOMELLI, U. & KIM, J. 1989 On the shape and dynamics of wall structures in turbulent channel flow. *Phys. Fluids* A**1**, 764.

JOHANSSON, A. V. & ALFREDSSON, P. H. 1982 On the structure of turbulent channel flow. *J. Fluid Mech.* **122**, 295.

JOHANSSON, A. V. & ALFREDSSON, P. H. 1983 Effects of imperfect spatial resolution on measurements of wall-bounded turbulent shear flows. *J. Fluid Mech.* **137**, 409.

JOHANSSON, A. V., ALFREDSSON, P. H. & ECKELMANN, H. 1987*a* On the evolution of shear-layer structures in near-wall turbulence. In *Advances in Turbulence, Proc. First European Turbulence Conference, Lyon, July 1986* (ed. G. Comte-Bellot & J. Mathieu). Springer.

JOHANSSON, A. V., ALFREDSSON, P. H. & KIM, J. 1987*b* Shear-layer structures in near-wall turbulence. In *Proc. First Summer Program of the Center for Turbulence Research, Rep.* CTR-S87. NASA Ames/Stanford University.

JOHANSSON, A. V., HER, A. V. & HARITONIDIS, J. H. 1987*c* On the generation of high amplitude pressure peaks in turbulent boundary layers and spots. *J. Fluid Mech.* **175**, 119.

KIM, J. 1985 Turbulence structures associated with the bursting event. *Phys. Fluids* **28**, 52.

KIM, H. T., KLINE, S. J. & REYNOLDS, W. C. 1971 The production of turbulence near a smooth wall in a turbulent boundary layer. *J. Fluid Mech.* **50**, 133.

KIM, J., MOIN, P. & MOSER, R. 1987 Turbulence statistics in fully developed channel flow at low Reynolds number. *J. Fluid Mech.* **177**, 133.

KLINE, S. J., REYNOLDS, W. C., SCHRAUB, F. A. & RUNSTADLER, P. W. 1967 The structure of turbulent boundary layers. *J. Fluid Mech.* **30**, 741.

KOBASHI, Y. & ICHIJO, M. 1986 Wall pressure and its relation to turbulent structure of a boundary layer. *Exps. Fluids* **4**, 49.

KOMORI, S., MURAKAMI, Y. & UEDA, H. 1989 Detection of coherent structures associated with bursting events in an open-channel flow by a two-point measuring technique using two laser-Doppler velocimeters. *Phys. Fluids* A **1**, 339.

KOVASZNAY, L. S. G., KIBENS, V. & BLACKWELDER, R. F. 1970 Large-scale motion in the intermittent region of a turbulent boundary layer. *J. Fluid Mech.* **41**, 283.

KREPLIN, H.-P. & ECKELMANN, H. 1979 Propagation of perturbations in the viscous sublayer and adjacent wall region. *J. Fluid Mech.* **95**, 305.

LANDAHL, M. T. 1990 On sub-layer streaks. *J. Fluid Mech.* **212**, 593.

LANGEHEINEKEN, T. 1981 Zusammenhänge zwischen Wanddruck- und Geschwindigkeitsschwankungen in turbulenter Rohrströmung. *Mitt. Max-Planck Institut für Strömungsforschung*, no. 70. Göttingen.

LIGRIANI, P. M. & BRADSHAW, P. 1987 Spatial resolution and measurement of turbulence in the viscous sublayer using subminiature hot-wire probes. *Exps. Fluids* **5**, 407.

LU, S. S. & WILLMARTH, W. W. 1973 Measurements of the structure of the Reynolds stress in a turbulent boundary layer. *J. Fluid Mech.* **60**, 481.

LUCHIK, T. S. & TIEDERMAN, W. G. 1985 Effect of spanwise probe volume length on laser velocimeter measurements in wall-bounded turbulent flows. *Exps. Fluids* **3**, 339.

PRANDTL, L. & TIETJENS, O. G. 1934 *Fundamentals of Hydro- and Aeromechanics.* Dover.

REYNOLDS, O. 1883 An experimental investigation of the circumstances which determine whether the motion of water shall be direct or sinous, and the law of resistance in parallel channels. *Phil. Trans. R. Soc. Lond.* **174**, 935.

ROBINSON, S. K., KLINE, S. J. & SPALART, P. R. 1989 Quasi-coherent structures in the turbulent boundary layer. Part II. Verification and new information from a numerically simulated flat-plate layer. In *Proc. Zoran Zaric Memorial Intl Seminar on Near-Wall Turbulence, May 1988 Dubrovnik.* Hemisphere.

SCHEWE, G. 1983 On the structure and resolution of wall-pressure fluctuations associated with turbulent boundary layer flow. *J. Fluid Mech.* **134**, 311.

SPALART, P. R. 1988 Direct numerical simulation of a turbulent boundary layer up to $Re_\theta = 1410$. *J. Fluid Mech.* **187**, 61.

WARK, C. E. 1988 Experimental investigation of coherent structures in turbulent boundary layers. Ph.D. thesis, Illinois Institute of Technology.

ZARIC, Z. 1972 Wall turbulence studies. *Adv. Heat Transfer* **8**, 285.